

[\[Print Version\]](#)
[\[PubMed Citation\]](#) [\[Related Articles in PubMed\]](#)

TABLE OF CONTENTS

[\[INTRODUCTION\]](#) [\[MATERIALS AND...\]](#) [\[RESULTS\]](#) [\[DISCUSSION\]](#) [\[CONCLUSIONS\]](#) [\[REFERENCES\]](#) [\[APPENDIX\]](#) [\[TABLES\]](#) [\[FIGURES\]](#)

The Angle Orthodontist: Vol. 70, No. 1, pp. 34-47.

Sliding Mechanics of Coated Composite Wires and the Development of an Engineering Model for Binding

Scott W. Zufall, BS, PhD;^a Robert P. Kusy, BS, MS, PhD^b

ABSTRACT

A tribological (friction and wear) study, which was designed to simulate clinical sliding mechanics, was conducted as part of an effort to determine the suitability of poly (chloro-*p*-xylylene) coatings for composite orthodontic archwires. Prototype composite wires, having stiffnesses similar to those of current initial and intermediate alignment wires, were tested against stainless steel and ceramic brackets in the passive and active configurations (with and without angulation). Kinetic coefficient of friction values, which were determined to quantify sliding resistances as functions of the normal forces of ligation, had a mean that was 72% greater than uncoated wire couples at 0.43. To improve analysis of the active configuration, a mathematical model was developed that related bracket angulation, bracket width, interbracket distance, wire geometry, and wire elastic modulus to sliding resistance. From this model, kinetic coefficients of binding were determined to quantify sliding resistances as functions of the normal forces of binding. The mean binding coefficient was the same as that of uncoated wire couples at 0.42. Although penetrations through the coating were observed on many specimens, the glass-fiber reinforcement within the composite wires was undamaged for all conditions tested. This finding implies that the risk of glass fiber release during clinical use would be eliminated by the coating. In addition, the frictional and binding coefficients were still within the limits outlined by conventional orthodontic wire-bracket couples. Consequently, the coatings were regarded as an improvement to the clinical acceptability of composite orthodontic archwires.

KEY WORDS: Binding, Coatings, Composites, Friction, Wire mechanics.

Accepted: September 1999. Submitted: April 1999.

INTRODUCTION [Return to TOC](#)

Fiber-reinforced polymer composites are currently being developed for use as orthodontic archwire materials.¹⁻²⁰ One incentive for this research is improved esthetics, since the translucent appearance of these wires tends to transmit the color of the teeth to which they are affixed.^{1,2} More important, however, is the capability to vary the stiffnesses of composite wires without changing cross-sectional profiles. This functional advantage over individual metallic wires would allow practitioners to use variable-modulus orthodontic techniques²¹ without having to change archwire materials as treatment progressed. Allergic reactions to nickel, which are a debatable concern for many metallic alloys, are also averted with composite materials.²²⁻²⁴ To date, studies designed to examine the mechanical properties,³ viscoelastic losses,⁴ water sorption,⁵ hydrolytic stability,⁶ sliding mechanics,⁷ and postprocessing formability (β -staging)⁸ of composite wires have shown strong support for their clinical viability. These studies have also inferred ways in which the current prototype wires could be improved.

An investigation of the frictional properties of composite wires against several orthodontic brackets showed that reinforcement fibers were abrasively worn from the wire surfaces when tests were conducted at high normal forces or angulations.⁷ This potential release of glass fibers within the oral cavity was considered unacceptable, and a polymeric surface coating was suggested as a potential remedy. The prerequisites for this coating material were that it be easily applicable in thin layers, be wear-resistant, and have low frictional characteristics. In addition, the coating material needed to be biocompatible and transparent. One material that exhibited all of these properties was poly(chloro-*p*-xylylene), which has been well established for use in biomedical-coating applications, such as catheters and cardiac pacemakers.^{25,26}

To determine the effects of poly(chloro-*p*-xylylene) surface coatings on archwire sliding mechanics, the tribological (friction and wear) characteristics of coated composite wires were evaluated. Three wires, having different stiffnesses, were tested against stainless steel, polycrystalline alumina, and single-crystal alumina brackets using a frictional testing apparatus that was designed to simulate clinical sliding mechanics. A mathematical model of the archwire-bracket system was also developed to facilitate data analysis of the active configuration (with angulation). Results were compared with previous work on the tribology of uncoated wires and with the frictional properties of several conventional wires.^{7,27} Although the coating increased sliding resistance, examination of the tested specimens showed that the coating protected the reinforcement fibers within the composite materials from damage at even the most extreme testing conditions. Since the frictional increase was within the limits outlined by conventional wires,²⁷ and given the perceived importance of containing reinforcement fibers, poly(chloro-*p*-xylylene) coatings were deemed an improvement to composite orthodontic archwires.

MATERIALS AND METHODS [Return to TOC](#)

Composite wires and bracket materials

The composite wires were made from S2-glass®, continuous-fiber yarns (493 S2 CG150 1/0 1.0Z, Owens Corning Corp, Toledo, Ohio) and a glassy copolymer matrix. Each yarn was composed of 204 glass filaments (9 μ m diameter) and was characterized by 1 axial rotation (twist) per inch of yarn length. The comonomer used for the matrix contained 61% (wt/wt) bisphenol-A diglycidyl methacrylate (Nupol 046-4005, Cook Composites and Polymers Co, North Kansas City, Mo) and 39% (wt/wt) triethylene glycol dimethacrylate (TEGDMA, Polysciences Inc, Warrington, Pa). Benzoin ethyl ether (BEE, Aldrich Chemical Co Inc, Milwaukee, Wis) was added (0.4% (wt/wt)) as the ultraviolet light-sensitive initiator for

polymerization. Straight wire specimens, having round cross-sectional profiles, were formed using a photo-pultrusion manufacturing technique.^{9,10} The stiffnesses of the wires were varied by changing the volume fraction of reinforcement (V_f) that was pultruded into the composite profiles. Wires having 3 different V_f values (Table 1) were fabricated with nominal cross-sectional diameters of 0.020 inches (0.51 mm) each. The V_f values were calculated using the number of reinforcement yarns and the cross-sectional areas of the precoated wires, the latter of which were determined from the mean of 8 diameter measurements (Sony μ -mate Digital Micrometer, Sony Magnescale America Inc, Orange, Calif).

The stainless steel (SS), polycrystalline alumina (PCA), and single-crystal alumina (SC) brackets each had a 0.022 in. (0.56 mm) slot width and no preangulation (Table 1). Two of the brackets (SS and PCA) had -7° of pretorque and the other bracket (SC) had 0° of pretorque.

Surface coating

Prior to coating, all archwire materials were washed with 95% ethanol to remove surface debris and air-dried in a class 100 clean room. Specimens were cut from the bulk material in 75 cm lengths and mounted in a rack that maintained a minimum separation of 5 mm between wires. The rack was sealed in a plastic wrap prior to removal from the clean room and shipped to an outside provider to be coated with a 10 μ m layer of poly(chloro-*p*-xylylene) (Parylene C—Specialty Coating Systems Inc, Indianapolis, Ind). After coating, all wire specimens were stored in the dark until testing to ensure that no ultraviolet degradation would occur.

The Parylene coating was applied using a 3-stage deposition procedure.²⁸ In the first stage, Parylene dimer was heated to approximately 150°C , which caused controlled sublimation to occur. The dimer vapor was transported by a vacuum pump to a second chamber and heated to approximately 680°C . At this temperature, the dimer broke down into Parylene monomer. The monomer was then moved into a deposition chamber that was kept at room temperature (25°C). Here, the monomer polymerized upon contact with any exposed surface, thereby coating the wire specimens.

Frictional testing

Frictional characteristics were measured using a device that was designed to simulate orthodontic sliding mechanics (Figure 1). This device and the associated testing procedure have been described elsewhere^{7,27} and are only briefly mentioned here. Each archwire-bracket combination (couple) was tested by mounting the bracket in the frictional testing device and connecting the wire to the load cell (50 kg scale) of a mechanical testing machine (Instron Model TTCM, Instron Corp, Canton, Mass). A computer-controlled normal force of ligation (N_{FR}) was applied through two 0.010 inch (0.25 mm) SS wires (Item PL 1010 Ligature Wire, GAC International, Commack, NY) to retain the archwire in the bracket slot (Figure 1c). (In previous work, the normal force of ligation was referred to as the “normal force” and was designated by N . The “FR” subscript has been added to this and other parameters to delineate between those that are associated with classical friction (FR) and those that are associated with binding (BI). See the first section of the Discussion.)

Bracket angulation (θ) was obtained by rotating the bracket and ligature wires with respect to the archwire (Figure 2). The transverse beam of the mechanical testing machine, to which the device was mounted, created a relative motion between the archwire and bracket.

In order to validate the frictional testing apparatus and its operator, a couple was tested and compared with prior results. Using the procedure that follows, an SS archwire (Standard Edgewise 0.021 inch \times 0.025 inch [0.53 mm \times 0.64 mm], American Orthodontics, Sheboygan, Wis) was tested at $\theta = 0^\circ$ and $N_{FR} = 0.2, 0.4, 0.6, 0.8,$ and 0.95 kg against a SS bracket. (Although SI units of force are conventionally expressed in newtons (N), grams (g) or kilograms (kg) are used almost exclusively in the orthodontic literature. Since 1 kg is approximately equal to 10 N, all measurements of force reported in this study can be thought of equivalently as either kg or dekanewtons (daN)). Analysis of the data, as described later, gave a kinetic coefficient of friction ($\mu_{k,FR}$) equal to 0.12, which was comparable to the results from previous frictional studies.^{27,29}

Prior to testing, all materials were rinsed in 95% ethanol to remove surface debris. Specimens of each composite archwire were tested against each of the brackets (Table 1) in the dry state at 34°C . When necessary to ensure that N_{FR} was applied normal to the floor of the bracket slot, brackets were mounted in the frictional testing apparatus on 7° inclines. Drawing forces (P) were measured with the Instron load cell as each bracket was translated a distance (δ) of 5 mm along an archwire at a sliding velocity of 10 mm/min. Each couple was sequentially tested at 12 different N_{FR} values ($N_{FR} = 0.05, 0.10, 0.15, 0.20, 0.25, 0.30, 0.075, 0.125, 0.175, 0.225, 0.275,$ and 0.40 kg) and 6 different θ values ($\theta = 0, 2.5, 5.0, 7.5, 10.0,$ and 12.5°) for a total of 648 individual tests. Virginal sections of archwire were used for each test, and new brackets and ligature wires were used for each unique value of θ .

Frictional data were analyzed using techniques described in the literature.^{7,27,29,30} The P data in the kinetic region of each test (Figure 3) were averaged and divided by 2 to obtain the resistances to sliding (RS) of the 9 archwire-bracket couples at each N_{FR} and θ . These data were plotted as a function of N_{FR} , and linear-regression coefficients were calculated for each RS- N_{FR} plot in the passive or active configurations (Figure 4). The $\mu_{k,FR}$ value for each couple at each θ was given by the slope of the regression line, and the portion of RS that was due to binding (BI) was given by the y-intercept.

Microscopic examination

After testing, selected archwire specimens were examined with a scanning electron microscope (SEM, Model JSM-6300FV, JEOL USA, Peabody, Mass) at 15 keV for any surface effects that were attributable to sliding. In addition, all tested wire specimens were examined under a stereo microscope (Spencer Stereoscopic Microscope, American Optical Company, Buffalo, NY) to evaluate the post test integrity of the Parylene C coating. This evaluation was made for each specimen on a pass or fail basis. Specimens that had no penetrations through the coating that exposed the underlying composite substrate were assigned a value of 1, and specimens with penetrations were assigned a value of 0.

Statistical analysis

All regression lines were evaluated using the probabilities (P) associated with the correlation coefficients (r) and the number of data points (n). The $\mu_{k,FR}$ and BI data were evaluated to indicate differences with respect to bracket material, V_f , and θ using multiple analysis of variance (MANOVA; SYSTAT Version 5, SYSTAT Inc, Evanston, Ill). Significant factors and interactions that were revealed using MANOVA were also examined using Tukey-Kramer pairwise comparisons. Contingency tables of the coating-integrity data were created for all combinations of each of the test factors: bracket material, V_f , N_{FR} , and θ . Independence was established using the Pearson chi-square statistic.³¹

RESULTS [Return to TOC](#)

Friction

The P - δ traces were often characterized by large P variations in the kinetic data region, especially as N_{FR} (Figure 3a) and θ (Figure 3b) were increased. However, several specimens tested at $\theta < 5^\circ$ had lower and sometimes less varied P magnitudes (Figure 3c). RS values were progressively less scattered with decreasing N_{FR} and θ (Figure 4a). As θ decreased, increases in the r values of the RS- N_{FR} regression lines were observed (Table 2). The slopes of these regression lines, which defined $\mu_{k,FR}$, varied from 0.10 to 0.65. The y-intercepts, which defined BI, varied from -0.04 kg to 0.24 kg. Increases in θ corresponded to proportional increases in BI (Table 2; Figure 4). All but 2 of the RS- N_{FR} correlations were statistically significant ($P < .05$), and most were highly significant ($P < .001$, Table 2).

Microscopy

Microscopic examinations of the tested archwire specimens revealed abrasive wear patterns in areas that had contacted the bracket or the ligature wires. Many of the specimens

were characterized by complete delamination of the Parylene C coating at the points of contact (Figure 5a). However, others exhibited discrete penetrations that were separated by sections of undamaged coating (Figure 5b), and several specimens were undamaged. These later specimens were the same wires that had been observed to have lower and less varied P magnitudes during frictional testing (Figure 3c). The severity of the coating damage increased with increasing N_{FR} and θ , and wear was greater at the wire-bracket interface than at the wire-ligature interface. No damage to the composite substrate, ie, no release of reinforcement fibers (Figure 5c), was observed on any of the Parylene C-coated wire specimens.

DISCUSSION [Return to TOC](#)

Archwire-bracket configuration

In studies of archwire-bracket sliding mechanics where θ is an independent variable, the data can usually be better examined by partitioning RS into several components. Looking first at the passive configuration, which has been defined as the condition where θ is less than some critical angle for binding (θ_c), RS results only from sliding contact between the wire and the floor and/or a side of the bracket slot (Figure 2a). In this case, RS is exclusively caused by classical friction (FR), which increases proportionally with N_{FR} at a rate described by $\mu_{k,FR}$ (Figure 4b). When θ equals or exceeds θ_c , however, RS is complicated by the addition of BI, which results from sliding contact between the wire and both sides of the bracket slot (Figure 2b). In this active configuration, the magnitude of BI increases proportionally with the normal force of binding (N_{BI}), which increases with θ . Ultimately, at higher values of θ , the wire is permanently deformed, and relative sliding motion may cease as notching (NO) occurs. Since NO represents an undesirable clinical condition, RS should generally be described in terms of FR and BI.

Statistical analyses

Statistical analyses of $\mu_{k,FR}$ revealed no significant differences with respect to bracket or V_f . Among all specimens tested, a highly significant ($P < .001$, $n = 54$) difference was only observed for $\theta = 12.5^\circ$. Since this represented an extreme value of θ , at which evidence of NO behavior was observed, the $\mu_{k,FR}$ values for $\theta = 12.5^\circ$ were omitted. The remaining data (Table 2) were grouped ($n = 45$) to obtain an overall mean $\mu_{k,FR}$ of 0.43 ± 0.10 for the Parylene C-coated composite (CC) wire couples.

Statistical analysis of the BI data revealed a highly significant ($P < .001$, $n = 54$) interaction between θ and V_f . Pairwise comparisons showed highly significant ($P < .001$, $n = 54$) differences for all values of θ tested except between values of 0° and 2.5° where BI values were consistently near zero (Table 2). This corresponded to the passive configuration at approximately $\theta \leq 2.5^\circ$. Differences in BI were also observed with respect to V_f for the C49 wires ($P < .001$). Since no other differences were observed, and since previous work with uncoated composite (UC) wires had shown that BI was affected by both θ and V_f , the data were grouped accordingly. The BI data were plotted as a function of θ for $\theta \geq 2.5^\circ$ (Figure 6), and regression analysis gave a highly significant ($P < .001$) line for each V_f . A hierarchical pattern was observed where the slope of the lines increased from 0.017 to 0.022 and 0.023 kg per degree as V_f increased for the C49, C59, and C70 wires, respectively.

Significant interactions were shown between coating integrity and both N_{FR} ($P < .002$) and θ ($P < .001$) by the Pearson chi-square statistical analysis (Table 3). The coating integrity was independent of both bracket and V_f .

Tribology of the passive configuration

Because the results of several previous studies were validated with the same aforementioned SS-SS couple, comparisons could be made with the present data. Of particular interest was how the present frictional properties compared to those of beta-titanium (β -Ti) and nickel titanium (NiTi) wires, since the CC wires have similar elastic moduli (E) and would likely be used in the same clinical situations. The properties of SS wires were also considered since SS-SS couples remain the low frictional standard of contemporary orthodontics.

The overall mean $\mu_{k,FR}$ of the CC wires was generally greater than the values reported for SS, β -Ti, and NiTi wires (Figure 7). MANOVA of the CC and UC data from a previous study revealed a significant ($P < .001$, $n = 99$) difference between $\mu_{k,FR}$ of the CC and UC wires. Assessment of the means showed that the coating caused a 72% increase in $\mu_{k,FR}$, which was unexpected since Parylene C has been reported to form low-friction surfaces.

For sliding friction, FR is often defined in terms of 3 mechanisms: the frictional resistances caused by shearing (SH_{FR}) of surface asperities, interlocking (IN_{FR}) of surface roughnesses, and plowing (PL_{FR}) of one surface by the other. With precision-engineered surfaces, such as metallic orthodontic wires and brackets, IN_{FR} and PL_{FR} can often be neglected. If one surface is substantially harder than the other, however, PL_{FR} tends to dominate sliding resistance as protrusions of the hard surface cause abrasive wear of the soft material.

Metals and ceramics are much harder than polymers. Consequently, for the CC wire-bracket couples, the bracket materials were all much harder than Parylene C. Analysis of the coating-integrity data indicated that as N_{FR} increased, the edges of the bracket slots tended to cut notches through the wire coating (Figure 5a,b; Table 3). Such wear patterns are characteristic of PL_{FR} . As NO behavior increased, more energy transfer was required to slide the wire as more of the coating was damaged or removed. This caused an increase in RS with N_{FR} , which in turn caused the higher-than-expected mean $\mu_{k,FR}$ value for the CC wires. Similar notching patterns have been observed on metallic wires, and NO-induced increases in sliding resistances have been demonstrated for epoxy-coated SS wires.

The effect of NO on FR, and consequently on RS, was particularly discernible on the specimens that exhibited stick-slip characteristics. A representative example of this behavior was shown by the P- δ trace (Figure 3c) and the notched wire surface (Figure 5b) of the C59-SS couple that was tested at $N_{FR} = 0.075$ kg and $\theta = 0^\circ$. (Recall from the statistical analysis of coating integrity in Table 3 that this wire could just as easily have been undamaged, as were 4 of the 9 wires tested at the same N_{FR} and θ .) The notched sections on this wire corresponded with the stick regions on the P- δ trace, and the undamaged sections corresponded with the slip regions. When the data for these regions were independently examined, P equaled 0.090 kg for the stick regions and 0.048 kg for the slip regions (Figure 3c). Additionally, one of the undamaged specimens had a P that was 0.02 kg. These observations suggest that sliding resistance could be substantially reduced by minimizing NO.

Tribology of the active configuration

From the previous discussion of wire-bracket configuration, the relationship between N_{BI} and BI is analogous to the relationship between N_{FR} and FR. The primary difference is that instead of being controlled directly, the magnitude of N_{BI} is controlled, at least in part, by the stiffness of the wire (given by the product of E and the area moment of inertia, I), the interbracket distance (IBD), the bracket width (WIDTH), θ , and θ_c . This lack of direct control makes frictional property comparisons in the active configuration more difficult than they are in the passive configuration. While $\mu_{k,FR}$ indicates the relative magnitude of FR that can be anticipated from any archwire-bracket couple, no equivalent coefficient exists to characterize the magnitude of BI. However, a model of the archwire-bracket system can be used to derive a mathematical relationship for N_{BI} in terms of stiffness (E - I), IBD, WIDTH, θ , and θ_c (Appendix 1). Using this relationship (equation A.24), a kinetic coefficient of binding ($\mu_{k,BI}$) can be determined from the slope of a BI vs N_{BI} plot. This outcome is analogous to the relationship among FR, N_{FR} , and their slope, $\mu_{k,FR}$.

An IBD of 19 mm was defined by the geometry of the frictional testing apparatus. For the CC wires, values of E were obtained from the literature,⁴ and the I value was calculated using nominal wire dimensions (Table 1, I = $3.32 \times 10^{-15} \text{ m}^4$). Using bracket and wire dimensions from the literature,^{27,46} a nominal WIDTH of 3.1 mm and a nominal θ_c of 1.1° were determined and used to calculate values of N_{BI} (Table 4). When the BI data were plotted with respect to N_{BI} , the 3 regression lines in Figure 6 collapsed into a single, highly significant ($P < .001$) line having a slope of 0.42 (Figure 8a), from which μ_{k-BI} was charted (Figure 8b). Values of N_{BI} and BI- N_{BI} linear regressions were similarly determined for UC (E and I were assumed the same as for CC wires) and metallic wires (E = 200, 68.9, and 33 GPa for SS, β -Ti, and NiTi wires, respectively; I = $8.03 \times 10^{-15} \text{ m}^4$).^{7,47} Because the investigators reported differences in the BI data for the various metal wire-bracket couples, each couple was analyzed separately. Although this limited the number of specimens for each regression (n = 4), all but 2 of the metal wire regression lines were statistically significant (Figure 8b).

A comparison of the μ_{k-BI} data showed that the CC wire values fell within the values calculated for the other wire materials. When coupled with SS brackets, values of μ_{k-BI} for the β -Ti and NiTi wires were highest, perhaps because of cold welding.^{30,48} In contrast, the μ_{k-BI} of the SS-SS couple was the lowest, which only appeared to contradict the high binding sensitivity previously attributed to these wires.^{27,34,49} In fact, μ_{k-BI} was low for SS because equation A.24, which defined N_{BI} , was implicitly normalized with respect to wire stiffness. Thus, for a given θ , BI was highest for SS wires. For a given countervailing couple, however, the μ_{k-BI} data suggests that BI was lowest for SS wires.

The μ_{k-BI} values for the CC and UC wires were nearly identical, and no differences were shown by the statistical analysis of the BI data. Given the difference in the μ_{k-FR} values of these wires, the similarity in their μ_{k-BI} values was puzzling.

As with FR, BI can also be broken down into shearing (SH_{BI}), roughness interlocking (IN_{BI}), and plowing (PL_{BI}) components.³⁷⁻⁴² Based on the previous discussion of tribological mechanisms in the passive configuration, PL_{BI} would be expected to dominate BI. Notches on the CC wires tested in the active configuration, which were like those observed in the passive configuration, supported this expectation.

For the UC wires, PL_{BI} -type behavior has been reported in the active configuration.⁷ The wear on these UC wire specimens, however, was different than the wear observed here for the CC wires in that NO occurred through the composite structure, rather than through a polymeric surface coating (Figures 5a, b vs Figure 5c). The differences in these 2 surfaces suggest some other mechanism, as perhaps differences in the depth of penetration, somehow equalized the energy transferred during sliding.

Observations of coating integrity indicated that the severity of plowing increased with θ (Table 3). The coating integrity data also showed an abrupt decrease to 0 for all $\theta \geq 7.5^\circ$, whereas the decrease associated with N_{FR} was more gradual. Since N_{BI} was less than 0.2 kg for the C49 wires at $\theta = 7.5^\circ$ (Table 4), the difference in this behavior could not be explained by differences in normal force magnitudes. However, N_{BI} was applied over a smaller area in the active configuration (part of the bracket slot side, Figure 2b) than N_{FR} was in the passive configuration (the entire bracket slot floor, Figure 2a). Consequently, the stress on the wire was greater, thereby increasing deformation of the coating. Thus, the sharp edges of the bracket slot dug further into the coating, increasing the severity of NO. Chamfering these slot edges could help reduce this behavior by making the load transition along the length of the wire more gradual,^{7,35,50} albeit at the expense of some loss of control.

CONCLUSIONS [Return to TOC](#)

The mathematical model of the orthodontic appliance incorporates important system parameters, such as wire stiffness and wire-bracket geometry, into the analysis of the active configuration. The equations ultimately provide a kinetic coefficient of binding (μ_{k-BI}), which is analogous to the kinetic coefficient of friction (μ_{k-FR}). This coefficient can be used to compare different wires and brackets based on the magnitudes of the countervailing couples they produce via angulation, rather than just on the magnitude of their angulation.

The increase in frictional resistance associated with Parylene C coatings should be considered within the context of the improvement in glass fiber containment. The μ_{k-FR} value for the coated wires is within the limits outlined by conventional archwire-bracket couples, and the release of glass fibers is eliminated by the coating. Additionally, since the binding coefficient was unchanged by the coating, the effect of the increase in the frictional coefficient on the total sliding resistance will be less at higher angulations. If the potential release of glass fibers in the oral cavity is considered unacceptable, as suggested in the introduction, then the overall impact of the coating is to improve the clinical acceptability of the composite wires.

Notching needs to be reduced in order to minimize frictional resistance. As this behavior was less frequent at lower normal forces, low ligation forces should be used with coated composite wires. Selecting orthodontic brackets designed with well-rounded slot edges may also help reduce notching and consequently improve clinical sliding mechanics.

ACKNOWLEDGMENTS

This study was supported by a biomedical research award from the American Association of Orthodontists Foundation (AAOF). We would also like to thank Unitek/3M and Sybron Dental Specialties for supplying the brackets, GAC International for supplying the ligation wires, and American Orthodontics for supplying the stainless steel archwires that were used in this study.

REFERENCES [Return to TOC](#)

1. Kusy RP. The Future of orthodontic materials: the long-term view. *Am J Orthod Dentofacial Orthop.* 1998; 113:91-95. [[PubMed Citation](#)]
2. Kobayashi M, Watari F, Imai T, Nakamura S. inventors; Sun Medical Co, Ltd, Rocky Mountain Morita Corporation, and Unitika Glass Fiber Co, Ltd, assignees. Esthetic orthodontic wire. US patent 5 759 029. June 2,1998.
3. Kennedy KC, Chen T, Kusy RP. Mechanical properties of micron-sized pultruded composite profiles. In: *Advanced Composites X. Proceedings of the 10th Annual ASM/ESD Advanced Composites Conference & Exposition.* Materials Park, Ohio: ASM International;. 1994:191-200.
4. Zufall SW, Kusy RP. Stress relaxation and recovery behavior of composite orthodontic archwires in bending. *Eur J Orthod.* 2000; 22: (12 pages in press).
5. Kennedy KC, Chen T, Kusy RP. Behavior of photopolymerized silicate-glass-fiber-reinforced dimethacrylate composites subjected to hydrothermal aging, part 1: steady-state sorption characteristics. *J Mater Sci Mater Med.* 1998; 9:243-248.
6. Kennedy KC, Chen T, Kusy RP. Behavior of photopolymerized silicate-glass-fiber-reinforced dimethacrylate composites subjected to hydrothermal aging, part 2: hydrolytic stability of mechanical properties. *J Mater Sci Mater Med.* 1998; 9:651-660.
7. Zufall SW, Kennedy KC, Kusy RP. Frictional characteristics of composite orthodontic archwires against stainless steel and ceramic brackets in the passive and active configurations. *J Mater Sci Mater Med.* 1998; 9:611-620.
8. Kennedy KC, Kusy RP. Investigation of dual-staged polymerization and secondary forming of photopultruded, fiber-reinforced, methacrylate-copolymer composites. *J Biomed Mater Res.* 1998; 41:549-559. [[PubMed Citation](#)]

9. Kennedy KC, Kusy RP. UV-cured pultrusion processing of glass-reinforced polymer composites. *J Vinyl & Additive Tech.* 1995; 1:182–186.
10. Kusy RP, Kennedy KC. inventors; University of North Carolina at Chapel Hill, assignee. Novel pultruded fiber-reinforced plastic and related apparatus and method. US patent 5 869 178. February 9, 1999.
11. Goldberg AJ, Burstone CJ. The use of continuous fiber reinforcement in dentistry. *Dent Mater.* 1992; 8:197–202. [[PubMed Citation](#)]
12. Jancar J, DiBenedetto AT. Thermoplastic fibre-reinforced thermoplastic composites for dentistry—part 1: hydrolytic stability of the interface. *J Mater Sci Mater Med.* 1993; 4:555–561.
13. Jancar J, DiBenedetto AT, Goldberg AJ. Fibre-reinforced composites for dentistry, part 2: effect of moisture on flexural properties of unidirectional composites. *J Mater Sci Mater Med.* 1993; 4:562–568.
14. Goldberg AJ, Burstone CJ, Hadjinikolaou I, Jancar J. Screening of matrices and fibers for reinforced thermoplastics intended for dental applications. *J Biomed Mater Res.* 1994; 28:167–173. [[PubMed Citation](#)]
15. Jancar J, DiBenedetto AT, Hadziinikolaou Y, Goldberg AJ, Dianselmo A. Measurement of the elastic modulus of fibre-reinforced composites used as orthodontic wires. *J Mater Sci Mater Med.* 1994; 5:214–218.
16. Karmaker AC, DiBenedetto AT, Goldberg AJ. Continuous fiber reinforced composite materials as alternatives for metal alloys used for dental appliances. *J Biomater App.* 1997; 11:318–328.
17. Kusy RP. A Review of contemporary archwires: their properties and characteristics. *Angle Orthod.* 1997; 67:197–208. [[PubMed Citation](#)]
18. Talass MF. inventor; Ormco Corporation, assignee. Orthodontic arch wire. US patent 4 869 666. September 26, 1989.
19. Goldberg AJ, Burstone CJ. Inventors; University of Connecticut, assignee. Orthodontic appliance system. US Patent 4 717 341. January 5, 1988.
20. Goldberg AJ, Burstone CJ. inventors; The University of Connecticut, assignee. Passive dental appliances of fiber-reinforced composites. US Patent 4 894 012. January 16, 1990.
21. Burstone CJ. Variable-modulus orthodontics. *Am J Orthod.* 1981; 80:1–16. [[PubMed Citation](#)]
22. Prystowsky SD, Allen AM, Smith RW, Nonomura JH, Odom RB, Akers WA. Allergic contact hypersensitivity to nickel, neomycin, ethylenediamine, and benzocaine. *Arch Derm.* 1979; 115:959–962. [[PubMed Citation](#)]
23. Jones TK, Hansen CA, Singer MT, Kessler HP. Dental implications of nickel hypersensitivity. *J Prosthet Dent.* 1986; 56:507–509. [[PubMed Citation](#)]
24. Al-Waheidi EMH. Allergic reaction to nickel orthodontic wires: a case report. *Quint Inter.* 1995; 26:385–387.
25. Parylene, a biostable coating for medical applications [company publication]. Indianapolis, Ind: Specialty Coating Systems Inc; 1994.
26. Stark N. Literature review: biological safety of parylene C. *Med Plastics Biomater.* 1996; March; 30–35.
27. Articolo LC, Kusy RP. Influence of angulation on the resistance to sliding in fixed appliances. *Am J Orthod Dentofacial Orthop.* 1999; 115:39–51. [[PubMed Citation](#)]
28. Parylene conformal coatings specifications and properties [company publication]. Indianapolis, Ind: Specialty Coating Systems Inc; 1996.
29. Kusy RP, Whitley JQ, Prewitt MJ. Comparison of the frictional coefficients for selected archwire-bracket slot combinations in the dry and wet states. *Angle Orthod.* 1991; 61:293–302. [[PubMed Citation](#)]
30. Kusy RP, Whitley JQ. Friction between different wire-bracket configurations and materials. *Semin Orthod.* 1997; 3:166–177. [[PubMed Citation](#)]
31. Sokal RR, Rohlf FJ. *Biometry*.. 3rd ed. New York, NY: WH Freeman and Company; 1995:369–385, 695–697, 724–743.
32. Kusy RP, Whitley JQ. Influence of archwire and bracket dimensions on sliding mechanics: derivations and determinations of the critical contact angles for binding. *Eur J Orthod.* 1999; 21:199–208. [[PubMed Citation](#)]
33. Nanda RS, Ghosh J. Biomechanical considerations in sliding mechanics. In: Nanda E, ed. *Biomechanics in Clinical Orthodontics*. Philadelphia, Pa: WB Saunders;. 1997:188-217.
34. Frank CA, Nikolai RJ. A comparative study of frictional resistances between orthodontic bracket and arch wire. *Am J Orthod.* 1980; 78:593–609.
35. Hansen JD, Kusy RP, Saunders CR. Archwire damage from ceramic brackets via notching. *Orthod Rev.* 1997; 11:27–31.
36. Articolo LC, Kusy K, Saunders CR, Kusy RP. Influence of ceramic and stainless steel brackets on the notching of archwires during clinical treatment. *Eur J Orthod.* In press.
37. Jastrzebski ZD. *The Nature and Properties of Engineering Materials*.. 2nd ed. New York, NY: John Wiley & Sons; 1976:182–185, 264.
38. Rabinowicz E. *Friction and Wear of Materials*.. 2nd ed. New York, NY: John Wiley & Sons; 1995:66–81, 105–112.
39. Gahr KZ. *Microstructure and Wear of Materials*.. Amsterdam: Elsevier; 1987. Tribology Series, No 10, 93–99.
40. Blau PJ. *Friction and Wear Transitions of Materials*.. Park Ridge, NJ: Noyes Publications; 1989:63–68, 134, 285–287.
41. Holmberg K, Matthews A. *Coatings Tribology; Properties, Techniques and Applications in Surface Engineering*.. Amsterdam, The Netherlands: Elsevier; 1994. Tribology Series, No 28, 37–42.
42. Czichos H. *Tribology; A Systems Approach to the Science and Technology of Friction, Lubrication and Wear*.. Amsterdam: Elsevier; 1986. Tribology Series, No 1, 73–81, 215–221.
43. Dickson JAS, Jones SP, Davies EH. A comparison of the frictional characteristics of five initial alignment wires and stainless steel brackets at three bracket to wire angulations: an in vitro study. *Br J Orthod.* 1994; 21:15–22. [[PubMed Citation](#)]
44. Beer FP, Johnston ER. *Mechanics of Materials*.. New York, NY: McGraw-Hill;. 1981:396-429.
45. Cernica JN. *Strength of Materials*.. 2nd ed. New York, NY: Holt, Reinhart, and Winston; 1966:220–223, 268–283.

46. Kusy RP, Whitley JQ. Assessment of second-order clearances between orthodontic archwires and bracket slots via the critical contact angle for binding. *Angle Orthod.* 1999; 69:71–80. [PubMed Citation]

47. Kusy RP, Greenberg AR. Effects of composition and cross section on the elastics properties of orthodontic archwires. *Angle Orthod.* 1981; 51:325–341. [PubMed Citation]

48. Kusy RP, Whitley JQ. Effects of surface roughness on the coefficients of friction in model orthodontic systems. *J Biomech.* 1990; 23:913–925. [PubMed Citation]


49. Peterson L, Spencer R, Andreasen G. A comparison of friction resistance for nitinol and stainless steel wire in edgewise brackets. *Quint Inter.* 1982; 13:563–571.

50. Tanne K, Matsubara S, Shibaguchi T, Sakuda M. Wire friction from ceramic brackets during simulated canine retraction. *Angle Orthod.* 1991; 61:285–290. [PubMed Citation]

51. Meriam LJ, Kraige LG. *Statics Engineering Mechanics*; vol 1. New York, NY: John Wiley & Sons; 1986:296–301.

APPENDIX 1 [Return to TOC](#)

Derivation of the normal force of binding

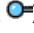
Derivation of the normal force of binding (N_{BI}) is perhaps best explained by starting with a classic problem. The kinetic coefficient of friction (μ_k) between a block and a plane can be experimentally determined by measuring the drawing force (P) required to initiate motion of the block. If P is measured parallel to the plane ([Appendix Figure A.1a](#) ) , then the normal force (N) between the block and the plane is equal and opposite to the mass of the block. Consequently, according to the first law of friction,^{37,51} μ_k is given by

$$\mu_k = \frac{P}{N} = \frac{P}{\text{Mass}}. \quad (\text{A.1})$$

If P is measured from below, instead of parallel to, the plane by the angle θ ([Appendix Figure A.1b](#) ) , then the component of P that is normal to the plane (given by $P \cdot \sin \theta$) is added to N , and μ_k is given by

$$\mu_k = \frac{P \cos \theta}{N} = \frac{P \cdot \cos \theta}{\text{Mass} + P \cdot \sin \theta}, \quad (\text{A.2})$$

where $P \cdot \cos \theta$ is the component of F that is parallel to the plane.

For an archwire-bracket couple in the active configuration, BI is measured at an angle (given by the difference between the bracket angulation, θ , and the critical binding angle, θ_c) with respect to N_{BI} ([Appendix Figure A.1c](#) ) . Thus the component of BI that is normal to the surface of the archwire (N_{P1}) will be summed with the force required to deflect the archwire (N_{P2}) such that

$$\mu_{k-BI} = \frac{BI \cdot \cos(\theta - \theta_c)}{N_{BI}} = \frac{BI \cdot \cos(\theta - \theta_c)}{N_{P1} + N_{P2}}, \quad (\text{A.3})$$

where $BI \cdot \cos(\theta - \theta_c)$ is the component of BI that is parallel to the surface of the archwire and

$$N_{P1} = BI \cdot \sin(\theta - \theta_c). \quad (\text{A.4})$$

Considering N_{P2} , the elastic curve of a prismatic beam can be modeled by the following differential equation:^{44, 45}

$$\frac{\frac{d^2y}{dx^2}}{\left[1 + \left(\frac{dy}{dx}\right)^2\right]^{3/2}} = \frac{M(x)}{E \cdot I}, \quad (\text{A.5})$$

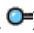
where M is the bending moment, E is the modulus of elasticity, and I is the area moment of inertia. For elastic deflections, the slope given by dy/dx is small, and the square of this term is generally considered to be negligible relative to unity. (This assumption is required in order to obtain a closed form solution to the differential equation A.5. As the curvature of the beam increases because of archwire-bracket angulation, changes in the interbracket distance, or changes in other parameters, this assumption may no longer be valid.) Thus, equation A.5 can be reduced to

$$\frac{d^2y}{dx^2} = \frac{M(x)}{E \cdot I}. \quad (\text{A.6})$$

In the active configuration, the bracket produces a mechanical couple that is normal to the wire surface and is separated by a moment arm equal to the mesiodistal width of the bracket (WIDTH) divided by $\cos(\theta_c)$ plus the size of the wire (SIZE) times $\sin(\theta_c)$. (This assumes that the bracket applies point forces at the mesial and distal edges of the bracket slot.)

However, for small values of θ_c , the moment arm can be approximated by

$$\text{moment arm} \approx \frac{\text{WIDTH}}{\cos(\theta_c)}. \quad (\text{A.7})$$

The mechanical couple can be resolved into a moment (M_0) applied at the center of a beam having a length (L ; [Appendix Figure A.2](#) ) . For this model, L is equal to twice the interbracket distance (IBD) minus WIDTH, where IBD is defined by the distance from the apical-coronal midline of one bracket to the apical-coronal midline of the next. Examining a portion of the beam, where $0 \leq x < (L/2)$, the equilibrium expression for the moments about an arbitrary point C is given by

$$\sum M_C = M_1(x) - (A_y \cdot x) + M_A = 0, \quad (\text{A.8})$$

where counterclockwise moments are assumed to be positive, A_y is the reaction force in the y-direction at the point A, M_A is the reaction moment at point A, and $M_1(x)$ is the moment at any point $0 \leq x < (L/2)$ in the beam. Solving for the bending moment at x gives

$$M_1(x) = (A_y \cdot x) - M_A. \quad (\text{A.9})$$

Similarly, for the remainder of the beam, where $(L/2) \leq x \leq L$, the equilibrium expression for the moments about an arbitrary point D is given by

$$\sum M_D = M_2(x) - (A_y \cdot x) + M_A + M_0 = 0, \quad (\text{A.10})$$

where counterclockwise moments are assumed to be positive.

Solving for the bending moment at x gives

$$M_2(x) = (A_y \cdot x) - M_A - M_0. \quad (\text{A.11})$$

By using a singularity function, these 2 equilibrium expressions can be combined into 1 equation:

$$M(x) = (A_y \cdot x) - M_A - M_0 \cdot \langle x - L/2 \rangle^0, \quad (\text{A.12})$$

where the singularity function is given by

$$\langle x - L/2 \rangle^n = \begin{cases} (x - L/2)^n & \text{when } x \geq L/2 \\ 0 & \text{when } x < L/2 \end{cases}$$

where $n = 0, 1, 2 \dots$ (A.13)

Assuming that the stiffness ($E \cdot I$) of the beam is constant along the length of the beam, equation A.12 can be substituted into equation A.6 to give

$$E \cdot I \cdot \frac{d^2y}{dx^2} = (A_y \cdot x) - M_A - M_0 \cdot \langle x - L/2 \rangle^0. \quad (\text{A.14})$$

Integrating twice with respect to x gives the relation for slope (dx/dy) and for deflection (y), respectively, as

$$E \cdot I \cdot \frac{dy}{dx} = \frac{A_y \cdot x^2}{2} - (M_A \cdot x) - (M_0 \cdot \langle x - L/2 \rangle^1) + C_1, \quad (\text{A.15})$$

$$E \cdot I \cdot y = \frac{A_y \cdot x^3}{6} - \frac{M_A \cdot x^2}{2} - \frac{M_0 \cdot \langle x - L/2 \rangle^2}{2} + (C_1 \cdot x) + C_2. \quad (\text{A.16})$$

The constants of integration in equations A.15 and A.16 can be determined by using the boundary conditions at $x = 0$ ([Appendix Figure A.2](#)) such that $C_1 = C_2 = 0$. The remaining unknown reactions can be determined using the boundary conditions at $x = L$. For equation A.16,

$$0 = \frac{A_y \cdot L^3}{6} - \frac{M_A \cdot L^2}{2} - \frac{M_0 \cdot \langle L - L/2 \rangle^2}{2}, \quad (\text{A.17})$$

$$A_y = \frac{3 \cdot M_A}{L} + \frac{3 \cdot M_0}{4 \cdot L}, \quad (\text{A.18})$$

which can be substituted into equation A.15. Solving equation A.15 for the remaining boundary condition results in

$$0 = \frac{3 \cdot M_A \cdot L^2}{2 \cdot L} + \frac{3 \cdot M_0 \cdot L^2}{8 \cdot L} - (M_A \cdot L) - \frac{M_0 \cdot L}{2}, \quad (\text{A.19})$$

$$M_A = \frac{M_0}{4}. \quad (\text{A.20})$$

Thus, the equations that model the elastic curvature of the beam are given by

$$E \cdot I \cdot \frac{dy}{dx} = M_0 \cdot \left(\frac{3 \cdot x^2 - (L \cdot x) - 4 \cdot L \cdot (x - L/2)^1}{4 \cdot L} \right), \quad (\text{A.21})$$

$$E \cdot I \cdot y = M_0 \cdot \left(\frac{2 \cdot x^3 - (L \cdot x^2) - 4 \cdot L \cdot (x - L/2)^2}{8 \cdot L} \right). \quad (\text{A.22})$$

Since the moment caused by a mechanical couple is the product of the magnitude of one of the forces (N_{P2}) times the distance between the forces (equation A.7), and since dy/dx at the center of the wire ($L/2$) is given by the tangent of $(\theta - \theta_C)$, equation A.21 can be solved for N_{P2} . Recalling that L is given by $(2 \cdot \text{IBD} - \text{WIDTH})$,

$$N_{P2} = \frac{16 \cdot E \cdot I \cdot \sin(\theta - \theta_C)}{\text{WIDTH} \cdot (2 \cdot \text{IBD} - \text{WIDTH})}, \quad (\text{A.23})$$

Thus, N_{BI} is given by summing N_{P1} and N_{P2} from equations A.4 and A.23, respectively:

$$\begin{aligned} N_{BI} &= N_{P1} + N_{P2} \\ &= \left(\frac{16 \cdot E \cdot I}{\text{WIDTH} \cdot (2 \cdot \text{IBD} - \text{WIDTH})} + BI \right) \cdot \sin(\theta - \theta_C). \end{aligned} \quad (\text{A.24})$$

TABLES [Return to TOC](#)

TABLE 1. Archwire and Bracket Materials

Material	Product	Code	Specifications
Archwires			
UFRP composite ^a	0.70 V_f^{bc}	C70	0.020 inch (0.51 mm) diameter
	0.59 V_f^{bc}	C59	0.020 inch (0.51 mm) diameter
	0.49 V_f^{bc}	C49	0.020 inch (0.51 mm) diameter
Brackets			
Stainless steel	Uni-Twin [®] Dyna-Lock ^{®d}	SS	0.022 inch (0.56 mm) slot, 0° angulation, -7° torque
Polycrystalline alumina	Transcend [®] Series 6000 ^d	PCA	0.022 inch (0.56 mm) slot, 0° angulation, -7° torque
Single-crystal alumina	Starfire [®] TMB ^e	SC	0.022 inch (0.56 mm) slot, 0° angulation, 0° torque

^a UFRP Composite, Unidirectional glass-fiber reinforced polymeric composite

^b V_f , Volume fraction of reinforcement

^c UNC Dental Research Center, Chapel Hill, North Carolina

^d Unitek/3M Corporation, Monrovia, California

^e Sybron Dental Specialties, Glendora, California

[®] Registered trademark

TABLE 2. Regression Analysis Summary From the Resistance to Sliding (RS) Versus Normal Force of Ligation (N_{FR}) Data of the Coated Composite Archwires^a

Bracket	Angulation $\theta(^{\circ})$	C70			C59			C49		
		μ_{k-FR}	BI (kg)	r	μ_{k-FR}	BI (kg)	r	μ_{k-FR}	BI (kg)	r
SS	0	0.38	-0.03	0.97	0.57	-0.02	0.98	0.59	-0.04	0.99
	2.5	0.37	0.01	0.90	0.41	-0.02	0.81	0.57	-0.04	0.98
	5.0	0.49	0.04	0.94	0.31	0.08	0.85	0.53	0.00	0.94
	7.5	0.33	0.14	0.92	0.39	0.12	0.92	0.37	0.06	0.69 ^b
	10.0	0.40	0.18	0.94	0.38	0.19	0.69 ^b	0.37	0.14	0.92
	12.5	0.14	0.23	0.86	0.31	0.22	0.85	0.15	0.16	0.73
PCA	0	0.56	-0.04	0.97	0.65	-0.04	0.98	0.45	-0.02	0.98
	2.5	0.52	0.00	0.98	0.56	-0.02	0.98	0.20	0.01	0.82
	5.0	0.55	0.03	0.95	0.40	0.02	0.77	0.49	0.03	0.95
	7.5	0.27	0.12	0.69 ^b	0.31	0.12	0.84	0.39	0.05	0.88
	10.0	0.36	0.17	0.78	0.54	0.15	0.95	0.58	0.11	0.96
	12.5	0.10	0.24	0.53 ^b	0.24	0.18	0.91	0.21	0.14	0.91
SC	0	0.40	0.00	0.99	0.35	-0.03	0.95	0.40	-0.01	0.98
	2.5	0.31	0.01	0.95	0.47	0.01	0.95	0.31	-0.01	0.96
	5.0	0.40	0.07	0.98	0.34	0.04	0.89	0.40	0.04	0.93
	7.5	0.46	0.12	0.99	0.50	0.09	0.90	0.46	0.06	0.96
	10.0	0.50	0.17	0.93	0.46	0.14	0.91	0.50	0.11	0.65 ^b
	12.5	0.44	0.24	0.87	0.25	0.22	0.80	0.44	0.19	0.29 ^c

^a Column headings are the kinetic coefficient of friction (μ_{k-FR}), binding (BI), and the regression correlation coefficient (r). All probabilities (P) associated with values of r and the number of data points ($n = 12$) were $P < .001$, except where indicated.

^b $P < .01$.

^c Not significant.

TABLE 3. Contingency Table of Coating Integrity for 648 Tests

Normal Force of Ligation, N_{FR} (kg)	Number of Intact Wire Specimens at Angulation, ^a $\theta =$						Total Specimens for Each N_{FR} ^b
	0°	2.5°	5.0°	7.5°	10.0°	12.5°	
0.050	6	3	0	0	0	0	9
0.075	4	4	1	0	0	0	9
0.100	3	2	0	0	0	0	5
0.125	4	3	1	0	0	0	8
0.150	2	0	0	0	0	0	2
0.175	3	2	1	0	0	0	6
0.200	1	1	0	0	0	0	2
0.225	2	2	1	0	0	0	5
0.250	2	0	0	0	0	0	2
0.275	1	2	0	0	0	0	3
0.300	0	0	0	0	0	0	0
0.400	0	1	0	0	0	0	1
Total specimens for each θ ^c	28	19	4	0	0	0	

^a $n = 9$ specimens for each θ versus N_{FR} cell.

^b $n = 54$ specimens for each N_{FR} cell.

^c $n = 108$ specimens for each θ cell.

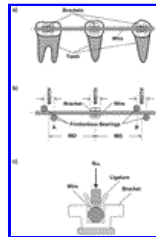
TABLE 4. Calculated Normal Force of Binding (N_{BI}) for the Coated Composite Archwires, Summarized by Wire Type^a

Archwire	Elastic Modulus, E (GPa) ^b	Angulation, θ (°)	Normal Force of Binding, N_{BI} (kg)
C70	62.4	0	0
		2.5	0.08
		5.0	0.22
		7.5	0.36
		10.0	0.52
		12.5	0.68
C59	49.5	0	0
		2.5	0.06
		5.0	0.17
		7.5	0.29
		10.0	0.41
		12.5	0.54
C49	37.5	0	0
		2.5	0.05
		5.0	0.13
		7.5	0.22
		10.0	0.31
		12.5	0.41

^a Data for the different bracket materials had a maximum difference of ± 0.01 kg for the N_{BI} values shown.

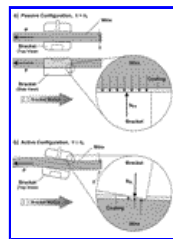
^b Elastic modulus data from reference 4.

FIGURES [Return to TOC](#)



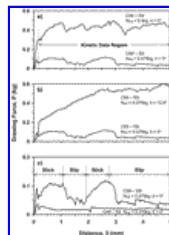
[Click on thumbnail for full-sized image.](#)

FIGURE 1. Schematics outlining the relationship between the dental physiology (a) and the frictional testing apparatus (b). Brackets to the left and right of the center bracket were each simulated using a pair of "frictionless" bearings. The normal force of ligation (N_{FR}) was applied (c) to simulate clinical ligation of the archwire



[Click on thumbnail for full-sized image.](#)

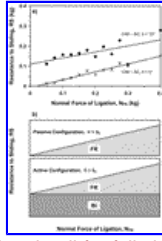
FIGURE 2. Schematics of an archwire-bracket couple in the passive (a) and in the active (b) configurations (adjacent brackets have been removed for clarity). When the bracket angulation (θ) was less than the critical angle for binding (θ_C), N_{FR} resulted from contact between the wire and the floor, and/or one side, of the bracket slot. When $\theta \geq \theta_C$, an additional normal force of binding (N_{BI}) resulted from contact between the wire and both sides of the bracket slot. Note that the contact area between the wire and the bracket was less on the side than on the floor of the bracket's slot. This implies that, when $N_{FR} = N_{BI}$, the stress on the side of the bracket's slot was greater, and consequently notching was more likely to occur at this location



[Click on thumbnail for full-sized image.](#)

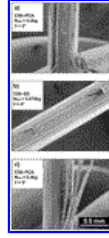
FIGURE 3. Traces of drawing force (P) versus distance (δ) for selected coated composite (CC) wire-bracket combinations. The kinetic data region delineates the data that were used

to calculate the resistance to sliding (RS), which equals $P/2$. Traces (a) and (b) show the effects of N and θ , respectively, on P . Trace (c) (note the change in y-axis scale) demonstrates the stick-slip behavior that was observed on several wire specimens, where the sticking regions correspond with two notches on the CC in Figure 5b. Trace (c) also shows the low P that was characteristic of samples undamaged during testing



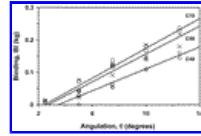
Click on thumbnail for full-sized image.

FIGURE 4. Regression lines through RS versus N_{FR} data for selected CC wires (a). Note how the increase in θ caused an upward shift between the RS- N_{FR} regression lines for $\theta = 0^\circ$ (\circ) and $\theta = 10^\circ$ (\bullet). Also shown is a schematic contrasting RS in the passive and in the active configurations (b).^{27,30,32} At $\theta < \theta_c$ the passive configuration exists (Figure 2a), and RS is caused only by classical friction (FR). When $\theta \geq \theta_c$ the active configuration exists (Figure 2b), and RS is caused by FR and binding (BI)



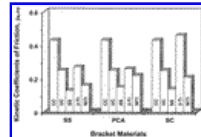
Click on thumbnail for full-sized image.

FIGURE 5. Scanning electron microscope (SEM) images of representative coated (a and b) and uncoated (c) C59 wires. Annotations indicate the wire, bracket, N_{FR} , and θ for each specimen. Note that the glass-reinforcement fibers of the composite were not damaged during sliding on the CC wires



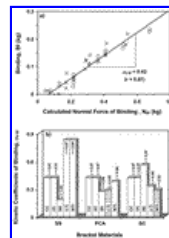
Click on thumbnail for full-sized image.

FIGURE 6. Regression lines through BI versus θ for the C49 (\diamond), C59 (\times), and C70 (\circ) CC wires (correlation coefficients, $r = 0.96, 0.97,$ and 0.99 , respectively). Note the slight differences in slope, which were associated with increases in wire stiffness



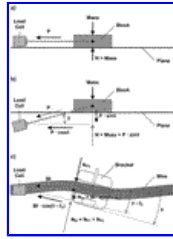
Click on thumbnail for full-sized image.

FIGURE 7. Comparison of the mean kinetic coefficients of friction ($\mu_{k,FR}$) for the CC wires with values from the literature for uncoated composite (UC), stainless steel (SS), beta-titanium (β -Ti), and nickel titanium (NiTi) wires against SS, polycrystalline alumina (PCA), and single-crystal alumina (SC) brackets.^{7,27}



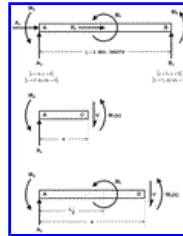
Click on thumbnail for full-sized image.

FIGURE 8. Regression line through BI versus the calculated normal force of binding (N_{BI}) data for all of the CC wires (a). The slope of this line, which represents the kinetic coefficient of binding ($\mu_{k,BI}$), equaled 0.42. This value was compared with values calculated from data in the literature for UC, SS, β -Ti, and NiTi wires against SS, PCA, and SC brackets (b).^{7,27} Although the sample size was small ($n = 4$), all but two values were significant (\circ). See Figure 6 for symbolic notations



Click on thumbnail for full-sized image.

FIGURE A.1. Schematic of an experiment for determining the kinetic coefficient of friction (μ_k) of a block against a plane (a and b). When the direction of the P required to initiate motion between the block and the plane changes from 0° (a) to some angle θ below the plane (b), the component of P that is normal to the plane is added to the mass of the block to obtain the normal force (N). Similarly, for the active configuration in archwire-bracket frictional testing (c), the component of BI that is normal to the wire (N_{P1}) is added to the force required to deflect the wire (N_{P2}) to obtain N_{BI} . Note that the adjacent bearings (Figure 1b) have been removed from the archwire-bracket schematic for clarity.



Click on thumbnail for full-sized image.

FIGURE A.2. Free-body diagrams of a wire-bracket couple from Figure 1b in the active configuration. The upper diagram simulates the reaction forces (A_y and B_y) and moments (M_A , M_B , and M_B) on the wire during frictional testing. The lower two diagrams simulate reaction forces at $0 \leq x < L/2$ and $L/2 \leq x \leq L$ in terms of shearing forces (V) and moments [$M_1(x)$ and $M_2(x)$] within the wire

^aDepartment of Biomedical Engineering, School of Medicine, University of North Carolina at Chapel Hill, Chapel Hill, NC.

^bDepartment of Biomedical Engineering, School of Medicine; Dental Research Center, School of Dentistry; Department of Orthodontics, School of Dentistry; Curriculum in Applied and Material Sciences, University of North Carolina at Chapel Hill, Chapel Hill, NC.

Corresponding author: Professor Robert P. Kusy, University of North Carolina at Chapel Hill, Dental Research Center, Building 210H, Room 313, CB#7455, Chapel Hill, NC 27599 (E-mail: rkusy@bme.unc.edu).